Supporting Information

Structure Evolution and Drying Dynamics in Sliding Cholesteric Cellulose Nanocrystals

Guang Chu, Rita Vilensky, Gleb Vasilyev, Patrick Martin, Ruiyan Zhang and Eyal Zussman*

NanoEngineering Group, Faculty of Mechanical Engineering, Technion-Israel

Institute of Technology, Haifa 32000, Israel

Corresponding Author:

meeyal@technion.ac.il

1. Materials and Apparatus

All Chemicals were used as received without further purification. Dimethylformamide (DMF, ≥99%, AR) were purchased from Sigma Aldrich. Cellulose nanocrystal (CNC) powder was obtained from the U.S. Forest Products Laboratory at University of Maine. The CNCs were prepared by controlled sulfuric acid hydrolysis and freeze-drying into solid powders.

Polarized optical microscopy (POM) image was conducted on Olympus BX51-P microscope with images taken by polarizers in a perpendicular arrangement to verify to the anisotropy of the composite samples. Videos were taken under the same microscope with a high-resolution DP74 camera (Olympus, resolution of 5760×3600 pixels) were used to record the motion of individual cholesteric fragment in suspension. Images were acquired with the frame rate up to 30 frames/s, at 200× magnification in cross-polarized state. Color videos with the resolution 1920×1200 and the frame rate 30 frames/s and 100×magnifications were used to acquire large-scale patterns of collective motion. Surface morphologies of the samples were characterized using a Zeiss Ultra Plus high-resolution scanning electron microscope (HR-SEM) at an accelerating voltage of 3 KV. Cryo-scanning electron microscopy (Cryo-SEM) was conducted on the same microscope equipped with a humidity chamber. Transmission electron microscopy (TEM) was conducted on a FEI Tecnai G2S-Twin with a field emission gun operating at 200 KV. Dynamic light scattering (DLS) measurements were conducted on Vasco Particle Size Analyzer. The measurements were performed at 173° scattering angle with 4 mW He-Ne laser

producing light with a wavelength of 633 nm. A Discovery DHR-2 rotational rheometer (TA Instruments, USA) was used to characterize the rheological properties of the suspension under steady-state shear flow. All rheological measurements were performed at room temperature (25 °C).

2. Experimental Section

Preparation of CNC in DMF suspension.

0.5 g CNC was dispersed into 7.8 ml DMF and stirred overnight, generating a visually homogeneous suspension with the CNC concentration of 6.0 wt%. After that, this suspension was sonicated for 15 min with ice bath and then standing for a varying time prior to drop-cast the suspension onto a glass slide. After standing for 2 days, the resulting suspension separated into two phases with the upper isotropic and bottom cholesteric phase.

Details for estimating the hydrodynamic shear stress.
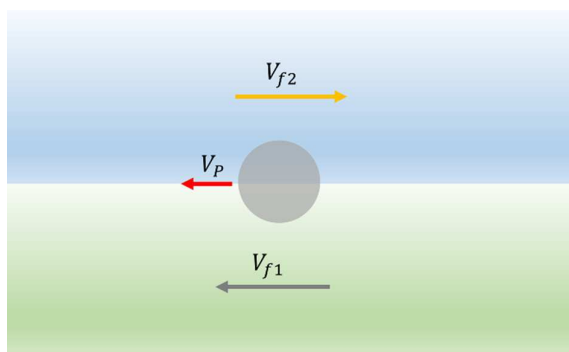
Scheme 1 Estimation of the hydrodynamic shear stress of the fragments during convective flow.

When a particle is moving during the flow, its hydrodynamic shear stress can be estimated as: $\tau \approx \eta \, {}^{\mu}\!/_{s}$.[1] Where τ is the shear stress, η is the viscosity of the fluid, μ is the relative velocity between fluid flow and the particle and s is the radius of the particle. For the CNC in DMF suspension, the zero shear viscosity is $\eta = 0.02 \, \text{Pa} \cdot \text{s}$ and the radius of the particle s is 40 μm. During the inward motion, the velocity of the particle is 35 μm/s and the velocity of the flow (V_{f1}) is 42 μm/s. Thus, the shear stress for inward is $\tau_1 \approx 0.02 \times {}^{(42-35)}\!/_{40} = 0.0035 \, Pa$. However, the outward flow also generate a shear stress for the particle at the same time. The outward flowing velocity (V_{f2}) is estimated as 30 μm/s. Due to the opposite moving direction, the shearing stress for outward is $\tau_2 \approx 0.02 \times {}^{(30+35)}\!/_{40} = 0.0325 \, Pa$. The shear stress for the particle is in a different magnitude with opposite direction, which results in hydrodynamic instability of the particle.

3. Supporting Movies

Supplementary Movie S1: The collective motion of CNC cholesteric fragments flowing from the drop centre to the contact line and then move back due to the Marangoni flow, showing flow-induced sliding instability.

Supplementary Movie S2: Rotating of the 3D cholesteric fragment during the flow, exhibiting structure transition, shape instability and inner orientation changing of the helical director.

Supplementary Movie S3: Folding of the 2D cholesteric fragment layer during the flow under hydrodynamic stress.

Supplementary Movie S4: The collective motion of CNC tactoids swimming from drop centre to the rim and then move back as evaporation progressed.

Supplementary Movie S5: CNC tactoids retained at contact line, and rotated during the convective flow.

Supplementary Movie S6: The cholesteric LC first move outward due to the capillary flow and then move inward due to the corresponding Marangoni flow, showing a convective laminar flow inside the whole drop. During the collective motion, the cholesteric ordering is totally destroyed by the shear stress but retained strong birefringence.

Supplementary Movie S7: The convective vortex flow of the cholesteric LC drop located at the edge of drop with symmetry distribution.

Supplementary Movie S8: The shifting of the convective flow from the drop edge to its interior due to the increase of viscosity and decrease of LC fluid motion as evaporation progressed.

Supplementary Movie S9: The collective motion of a large area of cholesteric LC ordering, showing typical fingerprint texture along the flow direction.

Supplementary Movie S10: The defect in cholesteric LC during the collective motion when the moving speed is low.

Note: All the videos are recorded and played at 30 fps.
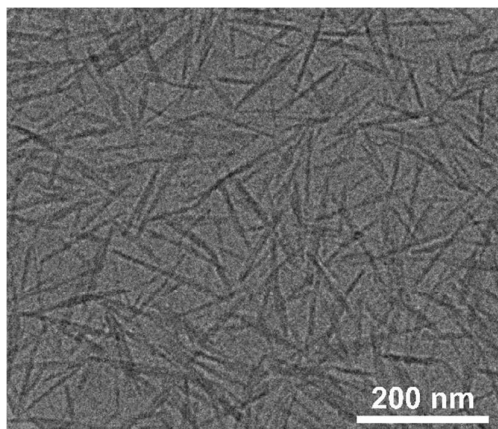
4. Supporting Figures

Figure S1 TEM image of the CNC prepared from a dilute suspension, which exhibits
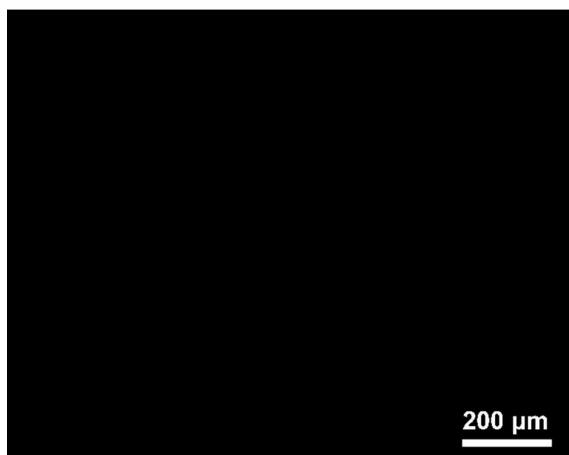
individual crystallites and rod-like morphology.

Figure S2 POM image of the CNC in DMF suspension just after sonication showing
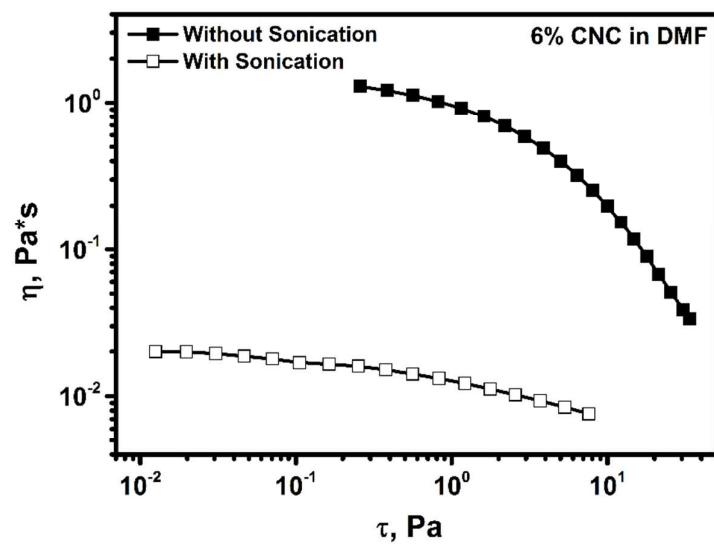
the isotropic property.

Figure S3 Viscosity variations of the CNC suspension with and without sonication.

Figure S4 Photograph of the 6.0 wt% (left) and 10.0 wt% CNC suspension after sonication which shows the concentration-dependent fluidity changes.
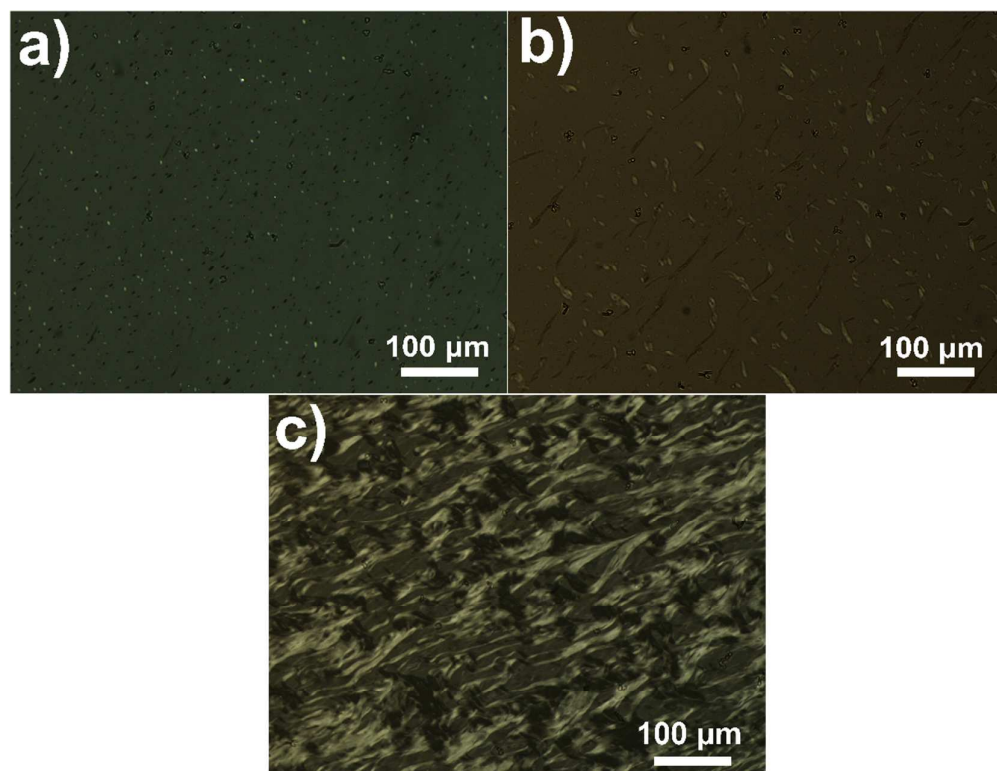
Figure S5 POM images of the growing of CNC aggregates from particles to one-dimensional birefringent filaments. 1h (a), 3h (b) and 5 h (c), respectively.
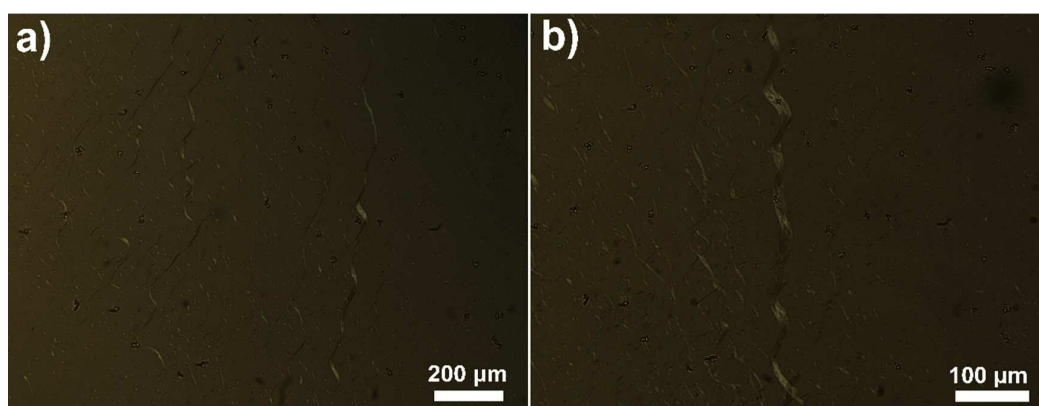
Figure S6 POM images of the twisted filaments of CNC with low (a) and high (b) magnification. The pitch of the filament is ~70 μm.
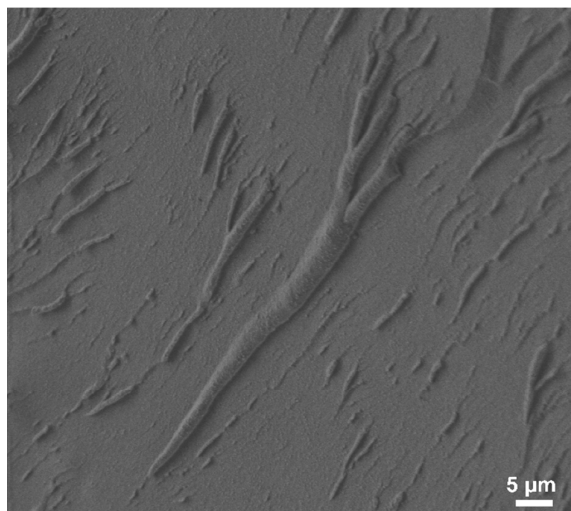
Figure S7 Cryo-SEM image of the cholesteric CNC fragment under low magnification.
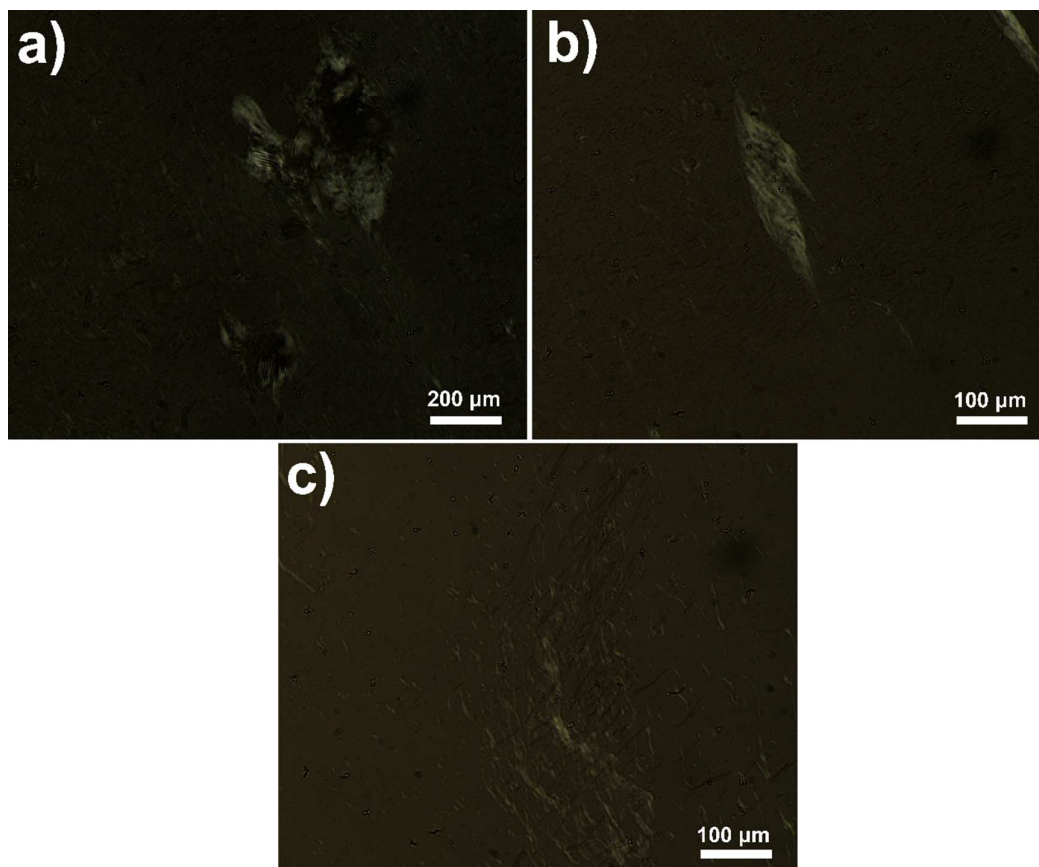
Figure S8 POM images of the cholesteric CNC fragment under high shear stress which exhibit the disassembly process of the fragment into bundles of twisted filaments.
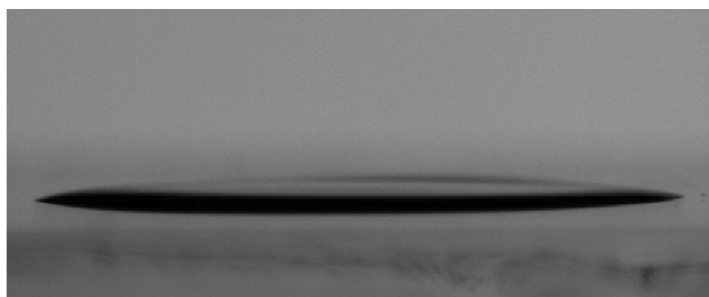
Figure S9 Photograph of an aged CNC suspension onto a glass slide. The contact line of the drop is pinned to the substrate with its contact angle of 15°.
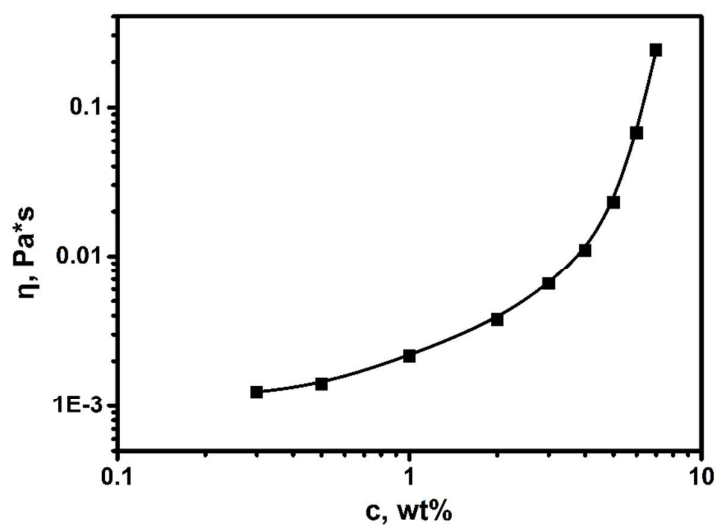

Figure S10 Concentration c versus the viscosity η measured at a constant shear rate of 10 s^{-1}. The viscosity of the CNC suspension increases with its corresponding concentration.
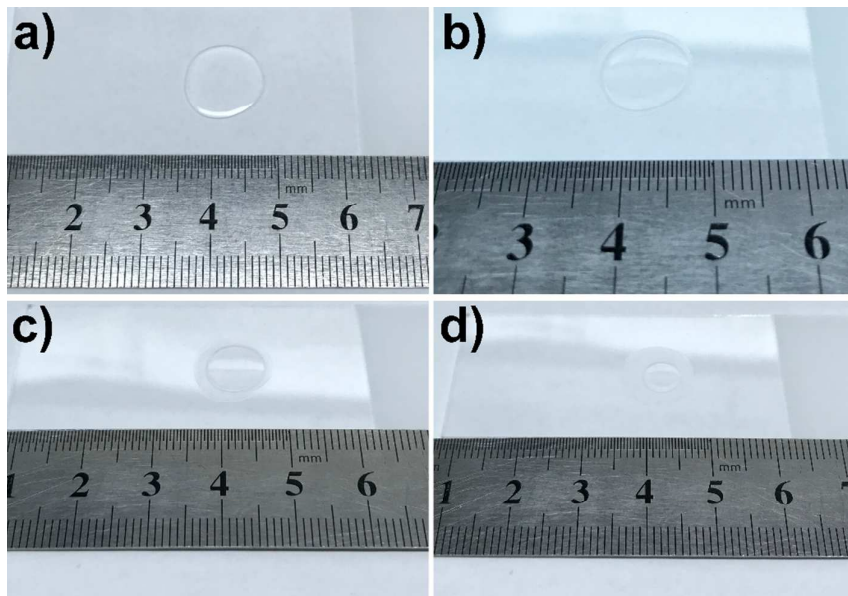
Figure S11 Photograph of the CNC suspension drop-casting onto a glass slide exhibits the retracting of the contact line. (a) 0h, (b) 1h, (c) 1.5h and (d) 2h, respectively.
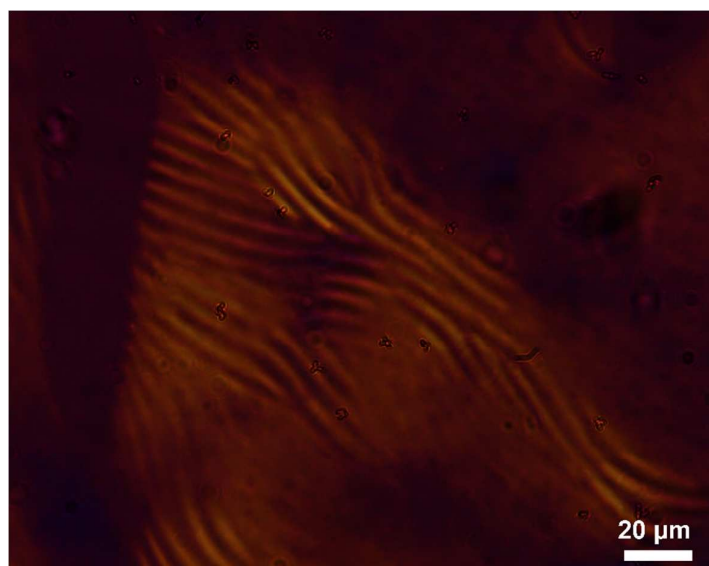

Figure S12 POM image of an individual CNC cholesteric fragment which shows topological defect inside it.
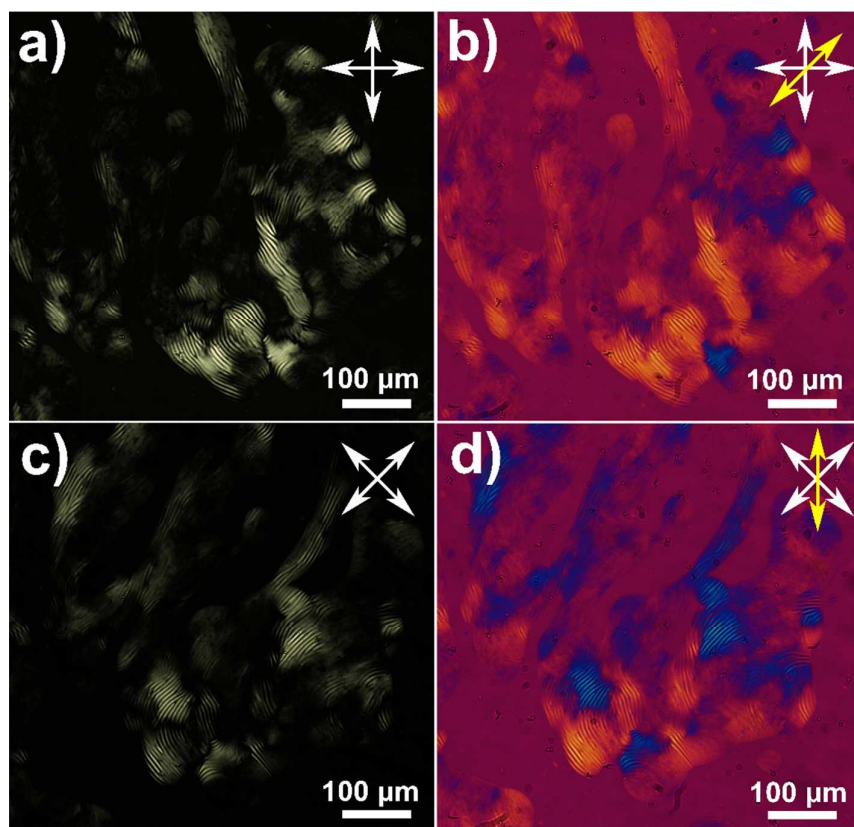
Figure S13 POM images of the CNC cholesteric fragment (a), (c) without and (b), (d) with a 530 nm retardation plate after rotating the sample for 45°.
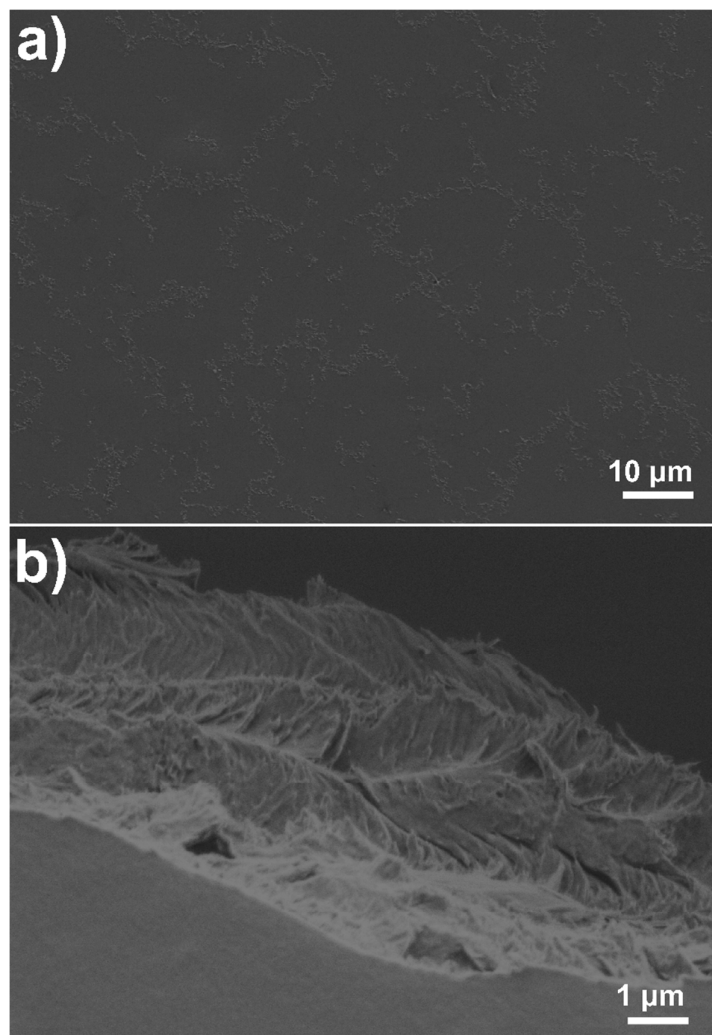
Figure S14 (a) SEM images of the drying CNC drop which exhibit the island distribute CNC fragment. (b) Zooming on a single island shows its chiral nematic arrangement of the CNC inside.
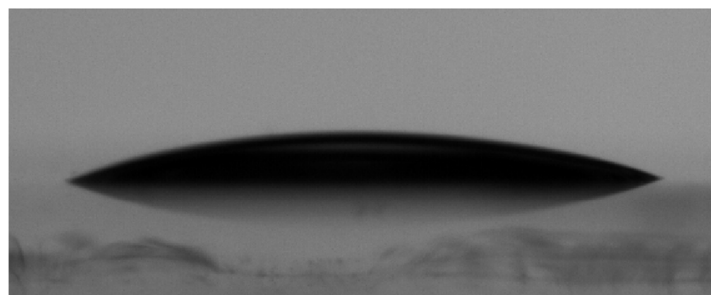

Figure S15 Image of pure cholesteric CNC phase onto a glass slide. The contact line

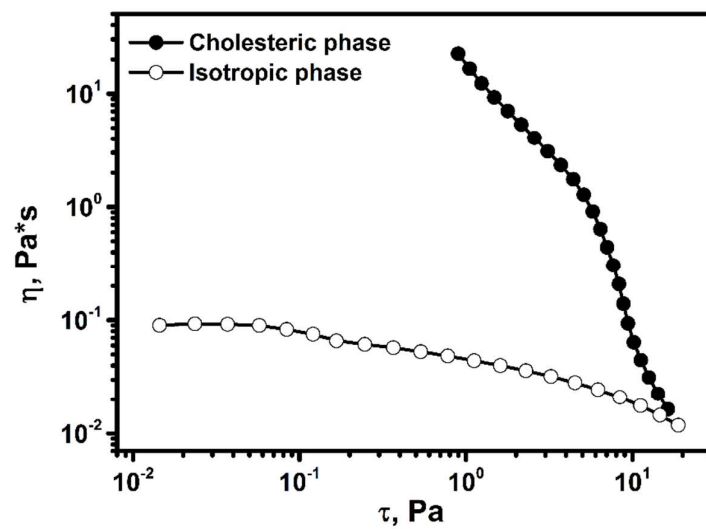of the drop is pinned to the substrate with its contact angle of 23°.

Figure S16 Viscosity variations of the CNC suspension with cholesteric phase and an
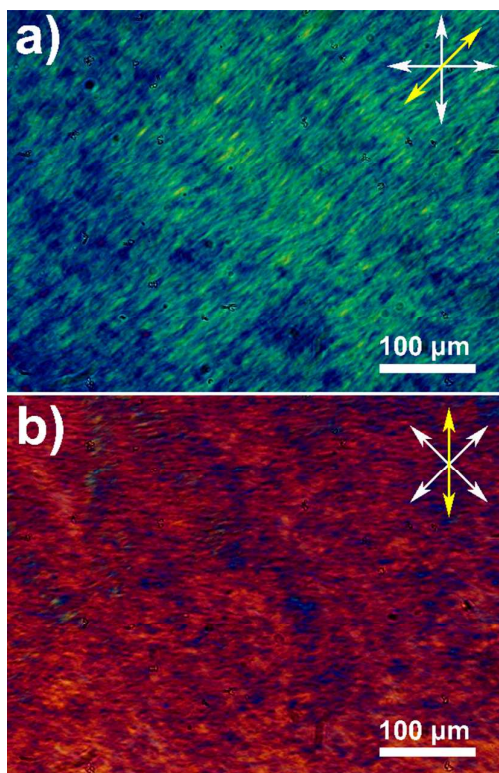
isotropic phase, respectively.

Figure S17 POM images of the flow inside the cholesteric drop before and after rotating 45° which indicate the high alignment of CNC during the flow.
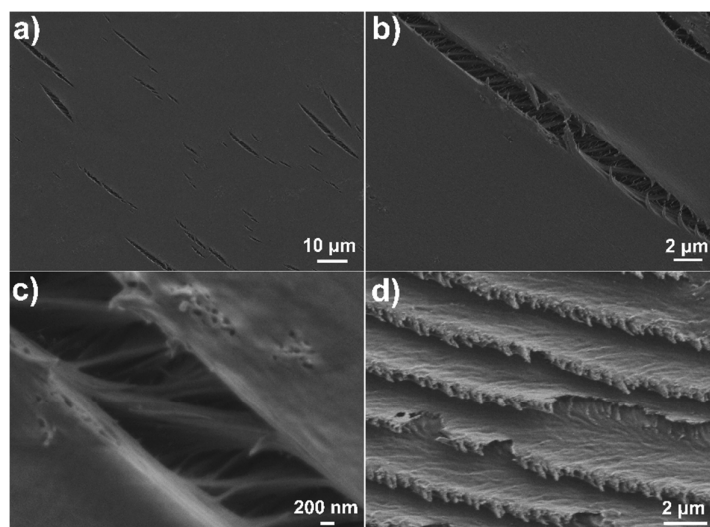

Figure S18 SEM images of the surface morphology for cholesteric CNC drop with different magnifications. (a) Low magnification of the surface of the cholesteric film which shows some cracks due to evaporation. (b) and (c) High magnification of the cracks in the film. Inside the crack, we can observe some periodic arrangement of CNC layer. (d) High magnification of the CNC layers inside the crack which exhibits typical cholesteric ordering with the helical structure lying perpendicularly to the substrate.

REFERENCE:

(1) Deegan, R. D.; Bakajin, O.; Dupont, T. F.; Huber, G.; Nagel, S. R.; Witten, T. A., Contact Line Deposits in an Evaporating Drop. *Phys. Rev. E* **2000**, *62*, 756.